Simulation on Flow and Heat Transfer in Diesel Particulate Filter

Kazuhiro Yamamoto[1]
e-mail: kazuhiro@mech.nagoya-u.ac.jp

Masamichi Nakamura

Department of Mechanical Science
and Engineering,
Nagoya University,
Furo-cho, Chikusa-ku,
Nagoya, Aichi 464-8603, Japan

To reduce particulate matters including soot, a diesel particulate filter (DPF) has been developed for the after-treatment of exhaust gas. Since the filter is plugged with particles that would cause an increase of filter back-pressure, filter regeneration process is needed. However, there is not enough data on the phenomena in DPF because there are many difficulties in measurements. In this study, the flow in DPF is simulated by the lattice Boltzmann method. To focus on a real filter, the inner structure of the filter is scanned by a 3D X-ray computed tomography technique. By conducting tomography-assisted simulation, the local velocity and pressure distributions in the filter can be visualized, which is hardly obtained by measurements. Results show that, even in cold flow, the complex flow pattern is observed due to the nonuniformity of pore structure inside the filter. Based on the flow characteristics in the range of 0.2–20 m/s, simulation results show a good agreement with the empirical equation of Ergun equation. In the combustion simulation, the time-dependent temperature field inside the filter is visualized. As the temperature of inflow gas is increased, the filter regeneration process is promoted.
[DOI: 10.1115/1.4003448]

Keywords: combustion and reactive flows, porous media, conduction, heat and mass transfer

1 Introduction

Since diesel engines have an advantage of lower fuel consumption, compared with gasoline engines, the amount of diesel car production in the world is gradually increased. However, there are more particulate matters (PMs) including soot in diesel exhaust gas. It is known that emission of soot particles can penetrate into the lung, causing human carcinogenic effects. Stricter exhaust emission standards, such as Euro V in 2008, are being set in many countries. Recently, a diesel particulate filter (DPF) has been developed for the after-treatment of exhaust gas. One of the common types of DPF is a monolithic wall-flow filter. Figure 1 is a photograph of a cordierite filter used in this study. In simple explanation of DPF, it traps PM when exhaust gas passes through its porous wall (Fig. 1(*b*)). It is the most efficient after-treatment device. It has been reported that DPF filtration efficiency can be as high as 99 % [1]. However, the filter is plugged with particles that would cause an increase of filter back-pressure, which must be kept at lower levels, because the higher back-pressure increases fuel consumption and reduces available torque [2]. Then, filter regeneration process is needed to oxidize accumulated particles.

So far, a continuously regenerating trap (CRT) [3,4] has been developed. Since it is passive regeneration, its process is spontaneously conducted during the normal engine operation. However, there is not enough data, and the phenomena occurring in the filter regeneration process are not well understood. This is because there are many difficulties in measurements. Typical inlet size of filter monolith is about 2 mm, and the thickness of the filter wall is only 0.2 mm, where soot particles are removed in the filter regeneration process. It is impossible to observe the small-scale phenomena inside the filter experimentally. Then, numerical simulation is a powerful tool to develop the after-treatment system such as catalytic converter [5].

In this study, the flow in a real DPF is simulated by lattice Boltzmann method (LBM). The structure of the cordierite filter is scanned by a 3D X-ray computed tomography (CT) technique. By conducting tomography-assisted simulation, it is possible to discuss local velocity and pressure distributions in the filter, which is hardly obtained by measurements. The soot combustion is included to examine the filter regeneration process. Here, the constant wall temperature is not assumed at the solid surface [6]. Instead, the heat transfer from the gas phase to the solid phase of the filter substrate is considered in simulations. This is because it could be an important factor to predict the temperature field in DPF more precisely. Based on simulation results, the heat and mass transfer inside the filter is discussed.

2 Numerical Approach

2.1 Lattice Boltzmann Method. To simulate the flow in the gas phase, the LBM is used. The fundamental idea of LBM is to construct simplified kinetic models that incorporate the essential physics of microscopic or mesoscopic processes so that the macroscopic averaged properties obey the desired macroscopic equations such as the N-S equations. The kinetic equation provides any of the advantages of molecular dynamics, including clear physical pictures, easy implementation of boundary conditions, and fully parallel algorisms [7]. LBM fulfills these requirements in a straightforward manner.

So far, many benchmark studies have been conducted. He and Doolen simulated the flow around two-dimensional circular cylinder to show the time evolution of vortex shedding [8]. As for the combustion simulation, the author and co-workers tested several flow geometries using LBM. For example, counterflow premixed flames have been simulated to confirm the validity of the proposed model [9]. It was the first lattice Boltzmann (LB) simulation on combustion, although coupled approach has been conducted to simulate flow field by LBM and temperature and concentration

[1]Corresponding author.

Contributed by the Heat Transfer Division of ASME for publication in the JOURNAL OF HEAT TRANSFER. Manuscript received November 2, 2009; final manuscript received September 12, 2010; published online March 4, 2011. Assoc. Editor: Mohamed-Nabil Sabry.

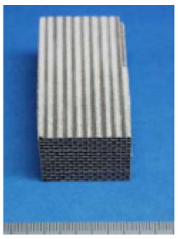

(a)

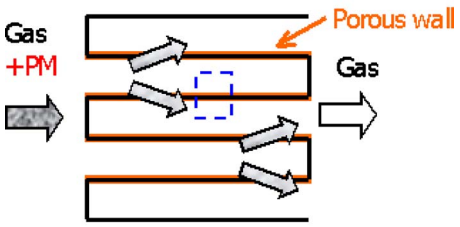

(b)

Fig. 1 (*a*) Photograph of cordierite filter and (*b*) PM trap inside porous filter wall. Calculation domain is shown by dotted line.

fields by a finite difference scheme [10]. To validate the LB simulation, the result has been compared with those by conventional method, solving differential conservation equations of mass, momentum, energy, and species. It has been demonstrated that the counterflow flame structure is well simulated, where both results are perfectly matched. In addition, the turbulent flames have been simulated using the conserved scholar approach [11]. The detailed chemistry and three-dimensional geometry were also tested by Yamamoto et al. [12]. It has been concluded that LBM can be used for combustion simulation.

Here, the numerical procedure is explained [9,11–14]. The flow is described by the lattice Bhatnagar-Gross-Krook (BGK) equation in terms of distribution function. Although 3D simulation is more suitable to consider the complex geometry of the filter, 2D simulation is conducted at first step. In Fig. 2, the 9 bit lattice BGK model evolves on the two-dimensional square lattice space with the following nine discrete velocities:

$$=(0,0) \quad (\alpha=0)$$

$$\boldsymbol{e}_\alpha=(\cos[(\alpha-1)\pi/2],\sin[(\alpha-1)\pi/2]) \times c \quad (\alpha=1-4)$$

$$=(\cos[(\alpha-5)\pi/2+\pi/4],\sin[(\alpha-5)\pi/2+\pi/4])\sqrt{2}\times c \quad (\alpha=5-8) \tag{1}$$

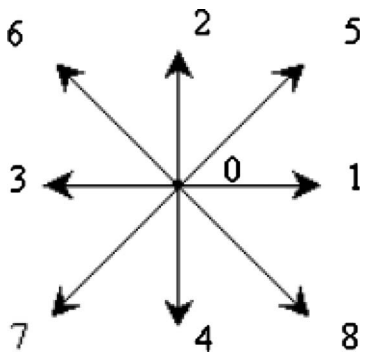

Fig. 2 D2Q9 model used in 2D simulation

where $c=\delta_x/\delta_t$, and δ_x and δ_t are the lattice constant and the time step, respectively. The evolution equation using the pressure distribution function is

$$p_\alpha(\boldsymbol{x}+\boldsymbol{e}_\alpha\delta_t,t+\delta_t)-p_\alpha(\boldsymbol{x},t)=-\frac{1}{\tau}[p_\alpha(\boldsymbol{x},t)-p_\alpha^{eq}(\boldsymbol{x},t)] \tag{2}$$

where τ is the relaxation time that controls the rate of approach to equilibrium. The equilibrium distribution function p_α^{eq} is given by

$$p_\alpha^{eq}=w_\alpha\left\{p+p_0\left[3\frac{(\boldsymbol{e}_\alpha\times\boldsymbol{u})}{c^2}+\frac{9}{2}\frac{(\boldsymbol{e}_\alpha\times\boldsymbol{u})^2}{c^4}-\frac{3}{2}\frac{\boldsymbol{u}\times\boldsymbol{u}}{c^2}\right]\right\} \tag{3}$$

where $w_0=4/9$, $w_\alpha=1/9$ $(\alpha=1-4)$, and $w_\alpha=1/36$ $(\alpha=5-8)$. The sound speed c_s is $c/\sqrt{3}$ with $p_0=\rho_0RT_0=\rho_0c_s^2$. Here, p_0 and ρ_0 are the pressure and density in the reference condition at temperature of 300 K and atmospheric pressure. To consider the variable density, the low Mach number approximation is adopted. The pressure and local velocity of $\boldsymbol{u}=(u_x,u_y)$ are obtained using the ideal gas equation.

$$p=\sum_\alpha p_\alpha \tag{4}$$

$$\boldsymbol{u}=\frac{\rho_0}{\rho}\frac{1}{p_0}\sum_\alpha \boldsymbol{e}_\alpha p_\alpha \tag{5}$$

The relaxation time is related with transport coefficients such as kinetic viscosity using $\nu=(2\tau-1)/6c^2\delta_t$. Through the Chapman–Enskog procedure, the Navier–Stokes equations are derived from these equations [7,15]. The LBM formula for temperature and concentration fields is

$$F_{s,\alpha}(\boldsymbol{x}+\boldsymbol{e}_\alpha\delta_t,t+\delta_t)-F_{s,\alpha}(\boldsymbol{x},t) =-\frac{1}{\tau_s}[F_{s,\alpha}(\boldsymbol{x},t)-F_{s,\alpha}^{eq}(\boldsymbol{x},t)]+w_\alpha Q_s, \quad s=T,Y_i \tag{6}$$

where Q_s is the source term due to chemical reaction. The equilibrium distribution function $F_{s,\alpha}^{eq}$ is given by

$$F_{s,\alpha}^{eq}=w_\alpha\times s\left\{1+3\frac{(\boldsymbol{e}_\alpha\times\boldsymbol{u})}{c^2}+\frac{9}{2}\frac{(\boldsymbol{e}_\alpha\times\boldsymbol{u})^2}{c^4}-\frac{3}{2}\frac{\boldsymbol{u}^2}{c^2}\right\} \tag{7}$$

Temperature T and mass fraction of species i, Y_i are determined by these distribution functions.

$$T=\sum_\alpha F_{T,\alpha} \tag{8}$$

$$Y_i=\sum_\alpha F_{Yi,\alpha} \tag{9}$$

2.2 Heat Transfer in Solid Phase. For modeling the filter regeneration process, the heat transfer from the gas phase to the solid phase of filter substrate is considered. Then, the following equation of heat conduction is solved:

$$\frac{\partial T}{\partial t}=\frac{\lambda}{\rho_s C_p}\left\{\frac{\partial^2 T}{\partial x^2}+\frac{\partial^2 T}{\partial y^2}\right\} \tag{10}$$

where λ, ρ_s, and C_p are the heat conductivity, density, and heat capacity of the filter. These values of cordierite filter are 1.9 W/m K, 2500 kg/m^3, and 1170 J/kg K. Needless to say, the convection and chemical reactions are not included in this equation. By coupling the equations in gas phase and using appropriate boundary conditions, the problem can be solved. It is assumed that the temperature and heat flux in the gas phase are equal to those in solid phase to determine the temperature at the

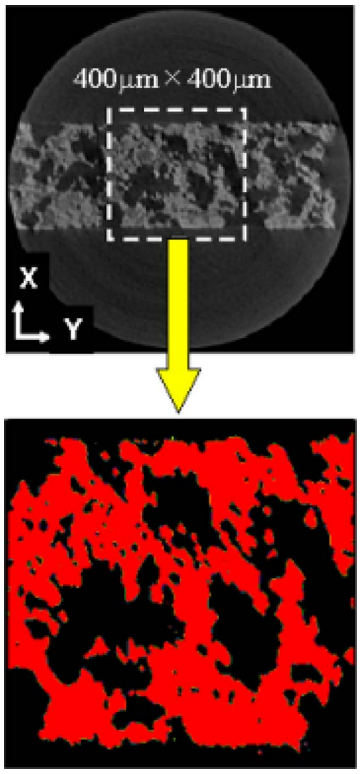

Fig. 3 Upper figure shows an example of X-ray CT images. Lower figure shows digitized data of dotted area. Complex porous structure with variety of pore size is well observed.

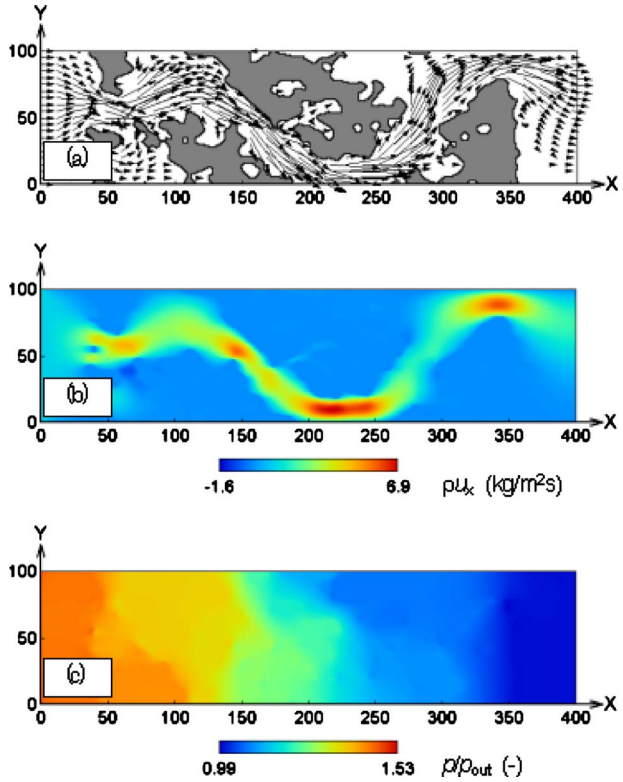

Fig. 4 Profiles of (*a*) flow across filter wall, (*b*) mass flux in *x*-direction, and (*c*) pressure. Inflow velocity in cold flow is 1 m/s. These profiles are obtained under steady state.

interface [16,17]. Other boundary conditions are explained in Sec. 2.3.

2.3 Calculation Domain and X-Ray CT Technique. To simulate the flow in the real diesel filter, the inner structure is obtained by a 3D X-ray CT technique [18–20]. Nondestructive nature of the CT technique allows visualization of filter inner structure actually used. The authors confirmed the applicability of the tomography-assisted simulation. In the present study, a similar data processing technique is employed.

Figure 3 shows a CT image of the filter, which was obtained in recent experiment [20]. Upper figure shows one example of the sliced filter, and lower figure shows digitized data used in simulation. The spatial resolution is 1 μm/pixel, which is the finest level in the reported CT measurements [16,17,21]. The dotted area is 400 μm(X)$\times$400 μm(Y). Complex porous structure with variety of pore size is well observed. Based on 3D CT data, it is found that the averaged porosity of filter is about 0.4. In the 2D simulation, one slice image of X-Y plane is used.

The calculation domain is 400×100 μm^2, and the grid number is $401(N_x)\times101(N_y)$. The grid size is 1 μm, which is the spatial resolution in X-ray CT measurement. To reduce the computational costs, an overall reaction by Lee et al. [22] is used in the soot oxidation (combustion). For simplicity, any catalytic effect is not considered. Inlet velocity and temperature of exhaust gas are changed.

As for the boundary condition, the inflow boundary is adopted at the inlet [23]. The gas component is of the diesel exhaust gas [20], and its temperature is changed to examine the filter regeneration process. The soot mass fraction is 0.05. At the sidewall, the slip boundary conditions are adopted, considering the symmetry [24]. At the outlet, the pressure is constant, and the gradient of scalar, such as temperature and mass fraction of species, is set to be zero. On the surface of the filter substrate, the nonslip boundary condition is adopted.

3 Results and Discussion

3.1 Flow Field. First of all, before simulating the filter regeneration process, the velocity and pressure profiles in the filter are examined. The cold flow at temperature of 300 K is used. Figure 4 shows the distribution of flow across the filter wall, nondimensional mass flux in x-direction, and pressure. The inlet velocity of U_{in} is 1 m/s. These profiles are obtained under steady state. It is found that the flow is forced to pass through the tunnel in pore structure of filter. Then, the pressure is gradually decreased along the flow direction. The velocity is locally accelerated in the narrow path near the exit. Although the calculation domain is relatively small, the flow characteristics inside the filter are captured in this simulation.

Next, the pressure field inside the filter is examined. The result is shown in Fig. 5. This pressure is the averaged value along the

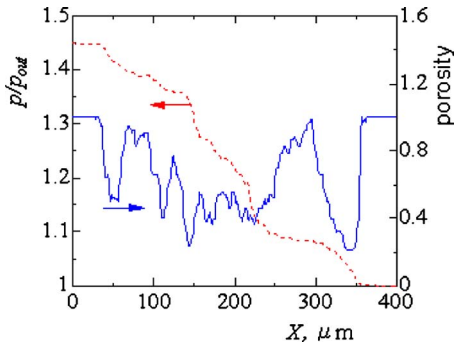

Fig. 5 Distributions of pressure and porosity across filter wall. Inflow velocity in cold flow is 1 m/s. These profiles are obtained under steady state.

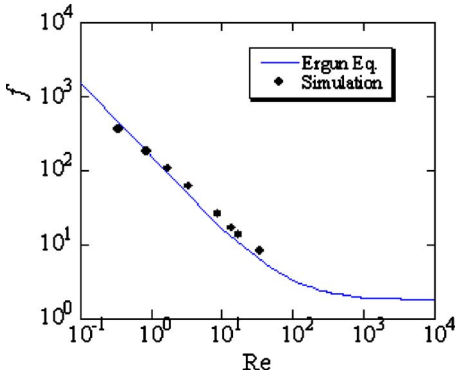

Fig. 6 Variations of friction factor with Reynolds number are shown, compared with the Ergun equation. Results in cold flow are shown under steady state.

Y-axis. For comparison, the porosity ε in this region is also shown. The filter wall is roughly located in the range of 30 μm $<X<370$ μm, and the porosity outside the filter is unity. It is well known that in the case of homogenous porous media, the pressure linearly decreases along the flow direction, and the pressure gradient is constant. However, as seen in this figure, since the porosity inside the filter wall is largely varied from 0.2 to 0.9, the pressure gradient is changed. Therefore, depending on the nonuniformity of pore structure, both flow and pressure are changed inside the filter.

Here, to confirm the validity of numerical scheme, simulation results are compared with the empirical equation. The idea is based on the porous media flow theory [25]. First, the hydraulic radius R_h and the equivalent diameter of the filter substrate D_p are determined.

$$R_h = \frac{\text{volume available for flow}}{\text{total wetted surface}} \tag{11}$$

$$D_p = 6R_h \frac{1-\varepsilon}{\varepsilon} \tag{12}$$

In experiments, the friction factor is determined by the streamwise pressure gradient [26]. Here, the friction factor f and Reynolds number Re are defined by

$$f = \left(-\frac{dp}{dx}\right)\frac{D_p}{\rho_0 U_{\text{in}}^2}\frac{\varepsilon^3}{(1-\varepsilon)} \tag{13}$$

$$\text{Re} = \frac{U_{\text{in}} D_p}{\nu(1-\varepsilon)} \tag{14}$$

The empirical equation, which is called an Ergun equation, is as follows:

$$f = 150/\text{Re} + 1.75 \tag{15}$$

Figure 6 shows simulation results. For comparison with the Ergun equation, cold and nonreactive flows are used. The inflow velocity is in the range of 0.2–20 m/s. It is found that, for all cases, a good agreement is observed. Although the computational domain is limited in the present tomography-assisted simulation, it is confirmed that the heat and mass transfer in the real filter could be discussed.

3.2 Soot Oxidation. Next, the soot oxidation process is simulated. Since the soot and oxygen are included in the inflow gas, the soot is automatically oxidized if the temperature is high enough. To initiate the reaction in the filter, the surface of filter substrate is heated at 1200 K. The mass fraction of soot is 0.05, and the temperature of inflow gas is changed. The oxygen volume concentration is 10% or 20%, and the inflow velocity is set to be 1 m/s.

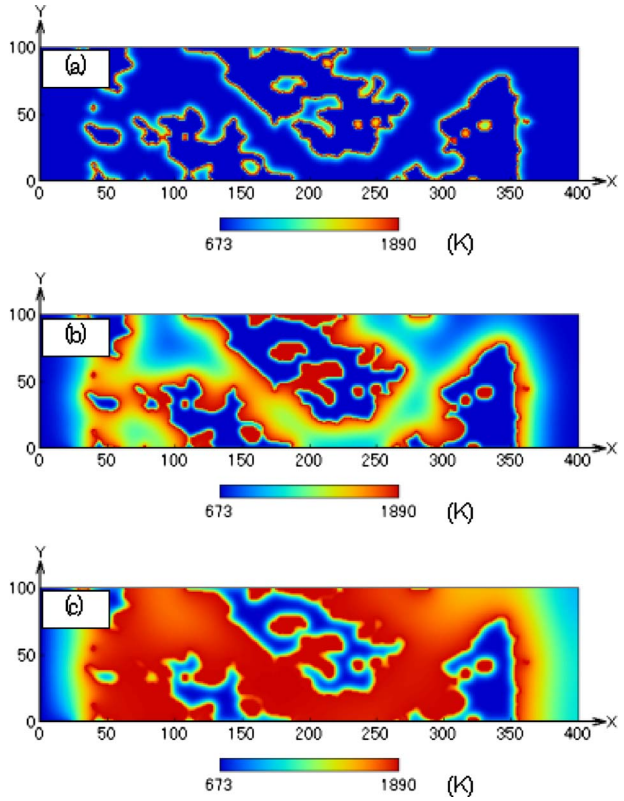

Fig. 7 Time variation of temperature profile: (*a*) t=0.1 μs, (*b*) t=2 μs, and (*c*) t=10 μs. Inflow velocity is 1 m/s, and mass fraction of soot is 0.05. Oxygen volume concentration is 10 %, and temperature of inflow gas is 673 K. It is observed that temperature only in gas phase is increased at the beginning.

Figure 7 shows the time variation of temperature profile. Time t is counted after the simulation is started. The temperature of inflow gas is 673 K, and the oxygen volume concentration is 10%. It is found that, at the beginning, only the temperature of gas phase is increased due to the soot oxidation. Then, the temperature of filter substrate is increased. The simulation is continued until the steady state is achieved. Figure 8 shows the distributions of temperature T (K), the mass fractions of soot and oxygen Y_C and Y_{O2}, and the reaction rate W_C(kg/m^3 s). The steady state is achieved at t=0.5 ms. It is found that the temperatures of gas phase and filter substrate are almost uniform. The soot concentration is decreased by the reaction with oxygen, and the reaction rate at the inlet is larger. Needless to say, the reaction rate locally varies, simply because the mass transfer of these reactants is different. In this condition, a part of soot is not oxidized inside the filter. That is, the filter regeneration process is not completed in this condition.

To examine the filter regeneration process, the temperature of inflow gas T_{in} is changed. Figure 9 shows the mass fraction of soot at the filter exit ($Y_{\text{C,exit}}$). The temperatures of inflow gas are 373 K, 673 K, and 973 K. The oxygen volume concentration is 20%. As seen in this figure, the soot concentration is gradually decreased along the flow direction. When the steady state is achieved, the soot concentration is almost constant at the filter exit. That is, the soot consumption is balanced with the soot supply in the inflow of exhaust gas. As the temperature is higher, the soot concentration at the filter exit is decreased, showing that more soot is oxidized in the filter. It is concluded that the present simulation demonstrates the capability of discussing the heat and mass transfer inside the filter.

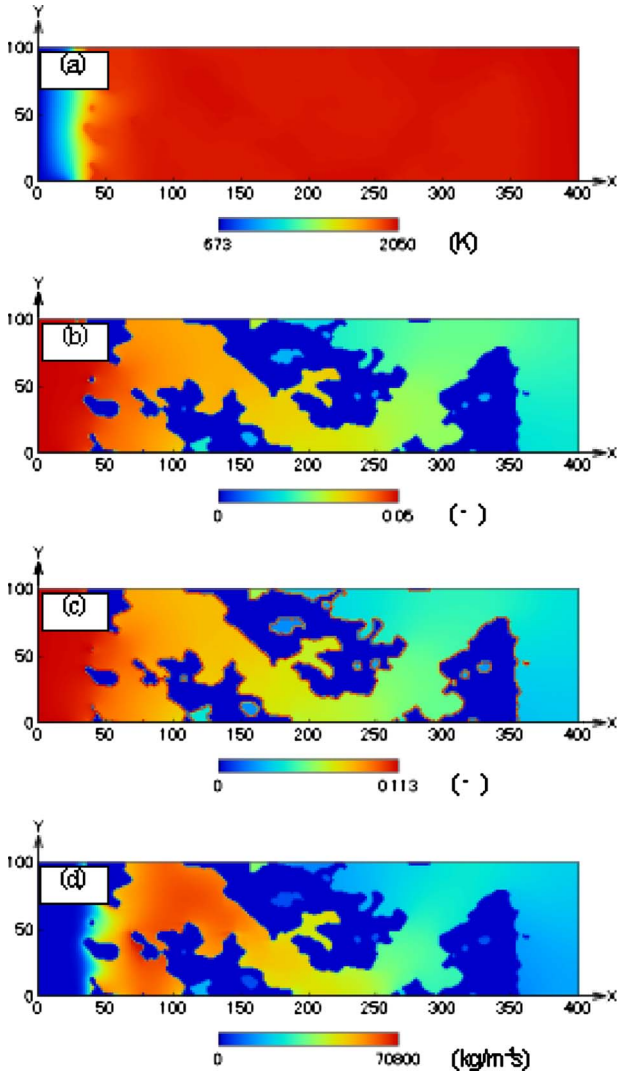

Fig. 8 Profiles of (*a*) temperature, (*b*) mass fraction of soot, (*c*) mass fraction of oxygen, and (*d*) reaction rate. Inflow velocity is 1 m/s, and mass fraction of soot is 0.05. Oxygen volume concentration is 10 %, and temperature of inflow gas is 673 K. These are obtained under steady state. Heat and mass transfer in soot oxidation is well visualized.

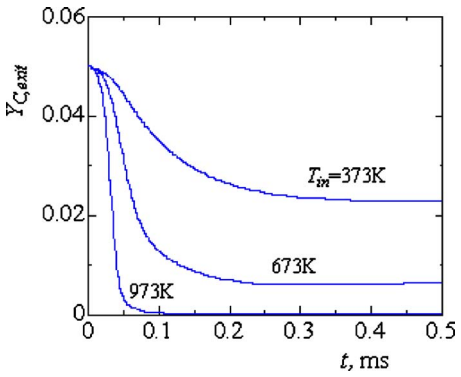

Fig. 9 Mass fraction of soot at filter exit is monitored. Inflow velocity is 1 m/s, and mass fraction of soot is 0.05. Oxygen volume concentration is 20 %, and temperature of inflow gas is varied from 373 K to 973 K. These are obtained under steady state.

4 Conclusions

In this study, the flow in the real cordierite filter by LBM has been simulated. The structure of the filter was scanned by the 3D X-ray CT technique. By conducting tomography-assisted simulation, the heat and mass transfer in the filter regeneration process have been discussed. In the numerical model, the heat transfer from the gas phase to the solid phase of the filter substrate was considered, which could be an important factor to predict the temperature field in DPF precisely. The following results are obtained.

(1) Even in cold flow, the complex flow pattern is observed due to the nonuniformity of pore structure inside the filter. Based on the flow characteristics in the range of 0.2–20 m/s, simulation results show a good agreement with the empirical equation of Ergun equation.
(2) In the simulation of soot oxidation process, the time-dependent temperature field inside the filter is visualized. At the beginning, only the temperature of gas phase is increased due to the soot oxidation. Then, the temperature of filter substrate is increased. Under the steady state, the temperature distribution inside the filter becomes almost uniform.
(3) As the temperature of inflow gas is increased, more soot is oxidized in the filter, showing that the filter regeneration process is promoted.

These are useful information to develop future on-board DPF system for the after-treatment of diesel exhaust gas.

Acknowledgment

This work was partially supported by the Grant-in-Aid for Scientific Research (C) in Japan (Grant No. 28560188).

Nomenclature

c = advection speed in LB coordinate
C_p = heat capacity of filter
D_p = equivalent diameter
e = unit vector for advection speed in LB coordinate
f = friction factor
$F_{p,\alpha}$ = distribution function of pressure
$F_{s,\alpha}$ = distribution function of T or Y_i
N = grid number
p = pressure
Q_s = source term by chemical reaction
R = ideal gas constant
Re = Reynolds number
R_h = hydraulic radius
s = scalar of temperature or species concentration
t = time
T = temperature
u = velocity vector
U_{in} = inlet velocity
W_C = reaction rate
x = direction normal to the filter
y = direction along the filter
Y_i = mass fraction of species I
ε = porosity
λ = heat conductivity of filter
ν = kinetic viscosity
ρ = density
ρ_s = density of filter
τ = relaxation time

Subscripts

0 = reference condition
C = properties of soot
exit = value at exit

in = value at inlet
s = properties of filter
α = number of advection speed in LB coordinate

References

[1] Searles, R. A., Bosteels, D., Such, C. H., Nicol, A. J., Andersson, J. D., and Jemma, C. A., 2002, "Investigation of the Feasibility of Achieving Euro V Heavy-Duty Emissions Limits With Advanced Emission Control Systems," FISITA 2002 World Congress, pp. 1–17, Paper No. F02E310.

[2] Stamatelos, A. M., 1997, "A Review of the Effect of Particulate Traps on the Efficiency of Vehicle Diesel Engines," Energy Convers. Manage., **38**(1), pp. 83–99.

[3] Cooper, B. J., Jung, H. J., and Toss, J. E., 1990, Treatment of Diesel Exhaust Gases, U.S. Patent No. 4,902,487.

[4] Hawker, P., 1995, "Diesel Emission Control Technology," Platinum Met. Rev., **39**, pp. 2–8.

[5] Arrighetti, C., Cordiner, S., and Mulone, V., 2007, "Heat and Mass Transfer Evaluation in the Channels of an Automotive Catalytic Converter by Detailed Fluid-Dynamic and Chemical Simulation," ASME J. Heat Transfer, **129**, pp. 536–547.

[6] Renksizbulut, M., and Niazmand, H., 2006, "Laminar Flow and Heat Transfer in the Entrance Region of Trapezoidal Channels With Constant Wall Temperature," ASME J. Heat Transfer, **128**, pp. 63–74.

[7] Chen, S., and Doolen, G. D., 1998, "Lattice Boltzmann Method for Fluid Flows," Annu. Rev. Fluid Mech., **30**, pp. 329–364.

[8] He, X., and Doolen, G. D., 1997, "Lattice Boltzmann Method on a Curvilinear Coordinate System: Vortex Shedding Behind a Circular Cylinder," Phys. Rev. E, **56**, pp. 434–440.

[9] Yamamoto, K., He, X., and Doolen, G. D., 2002, "Simulation of Combustion Field With Lattice Boltzmann Method," J. Stat. Phys., **107**(1/2), pp. 367–383.

[10] Filippova, O., and Haenel, D., 2000, "A Novel Numerical Scheme for Reactive Flows at Low Mach Numbers," Comput. Phys. Commun., **129**, pp. 267–274.

[11] Yamamoto, K., 2003, "LB Simulation on Combustion With Turbulence," Int. J. Mod. Phys. B, **17**(1–2), pp. 197–200.

[12] Yamamoto, K., He, X., and Doolen, G. D., 2004, "Combustion Simulation Using the Lattice Boltzmann Method," JSME Int. J., Ser. B, **47**(2), pp. 403–409.

[13] Yamamoto, K., and Ochi, F., 2006, "Soot Accumulation and Combustion in Porous Media," J. Energy Inst., **79**, pp. 195–199.

[14] Yamamoto, K., and Takada, N., 2006, "LB Simulation on Soot Combustion in Porous Media," Physica A, **362**, pp. 111–117.

[15] He, X., and Luo, L.-S., 1997, "Lattice Boltzmann Model for the Incompressible Navier–Stokes Equation," J. Stat. Phys., **88**(3/4), pp. 927–944.

[16] Petrasch, J., Schrader, B., Wyss, P., and Steinfeld, A., 2008, "Tomography-Based Determination of the Effective Thermal Conductivity of Fluid-Saturated Reticulate Porous Ceramics," ASME J. Heat Transfer, **130**, p. 032602.

[17] Haussener, S., Coray, P., Lipiński, W., Wyss, P., and Steinfeld, A., 2010, "Tomography-Based Heat and Mass Transfer Characterization of Reticulate Porous Ceramics for High-Temperature Processing," ASME J. Heat Transfer, **132**, p. 023305.

[18] Yamamoto, K., Satake, S., Yamashita, H., Takada, N., and Misawa, M., 2006, "Lattice Boltzmann Simulation on Porous Structure and Soot Accumulation," Math. Comput. Simul., **72**, pp. 257–263.

[19] Yamamoto, K., Takada, N., and Misawa, M., 2005, "Combustion Simulation With Lattice Boltzmann Method in a Three-Dimensional Porous Structure," Proc. Combust. Inst., **30**, pp. 1509–1515.

[20] Yamamoto, K., Oohori, S., Yamashita, H., and Daido, S., 2009, "Simulation on Soot Deposition and Combustion in Diesel Particulate Filter," Proc. Combust. Inst., **32**, pp. 1965–1972.

[21] Haussener, S., Lipiński, W., Petrasch, J., Wyss, P., and Steinfeld, A., 2009, "Tomographic Characterization of a Semitransparent-Particle Packed Bed and Determination of Its Thermal Radiative Properties," ASME J. Heat Transfer, **131**, p. 072701.

[22] Lee, K. B., Thring, M. W., and Beer, J. M., 1962, "On the Rate of Combustion of Soot in a Laminar Soot Flame," Combust. Flame, **6**, pp. 137–145.

[23] He, X., Chen, S., and Doolen, G. D., 1998, "A Novel Thermal Model for the Lattice Boltzmann Method in Incompressible Limit," J. Comput. Phys., **146**, pp. 282–300.

[24] Inamuro, T., Yoshino, M., and Ogino, F., 1999, "Lattice Boltzmann Simulation of Flows in a Three-Dimensional Porous Structure," Int. J. Numer. Methods Fluids, **29**, pp. 737–748.

[25] Bird, R. B., Stewart, W. E., and Lightfoot, E. N., 1960, *Transport Phenomena*, Wiley, New York.

[26] Burgess, N. K., and Ligrani, P. M., 2005, "Effects of Dimple Depth on Channel Nusselt Numbers and Friction Factors," ASME J. Heat Transfer, **127**, pp. 839–847.